Lasers in Surgery and Medicine 26:364–375 (2000)

Laser-Induced Shock Wave Endothelial Cell Injury

Anders Sondén, MD,[1]* Bengt Svensson, MD,[2] Nils Roman, MsC,[3] Henric Östmark, PhD,[3] Bo Brismar, MD, PhD,[4] Jan Palmblad, MD, PhD,[5] and B. Thomas Kjellström, MD, PhD[3]

[1]*Department of Anesthesiology and Intensive Care, Huddinge University Hospital, S-141 86 Huddinge, Sweden*
[2]*Department of Ophthalmology, University Hospital, S-901 85 Umeå, Sweden*
[3]*Defense Research Establishment, S-172 90 Stockholm, Sweden*
[4]*Division of Emergency Medicine, Huddinge University Hospital, S-141 86 Huddinge, Sweden*
[5]*Department of Hematology, Huddinge University Hospital, S-141 86 Huddinge, Sweden*

Background and Objective: **Several laser procedures, extracorporeal lithotripsies (ESWL), and high-velocity missile trauma generate pressure transients that are transmitted through the tissues. Despite several publications demonstrating shock wave–induced tissue injury, little is known about its pathophysiology. This study introduces an in vitro model for studying shock wave effects on endothelial cell (EC) monolayers.**
Study Design/Materials and Methods: **A Nd:YAG laser-driven flyer-plate technique was used to generate shock waves. Physical characteristics were determined with a pressure transducer, a high-speed video camera, and sequential photography. Biological effects were studied with phase contrast and lightfield microscopy, computerized morphometry, immunocytochemistry, spectrophotometry, and enzyme-linked immunosorbent assay (ELISA).**
Results: **The shock waves generated were highly reproducible. Cavitation was verified and quantified, and its extent could be varied in the vials. Exposed cultures exhibited areas with cell membrane damage and cell detachment. Release of LD was elevated ($P < 0.01$) in exposed vials. The EC lesions were larger ($P < 0.01$) in cultures submitted to high vs. low extent of cavitation.**
Conclusion: **The flyer-plate model can be used to subject cell monolayers to defined and reproducible shock waves causing immediate cell injury similar to the previously reported vascular lesions associated with ESWL, pulsed lasers, and blast trauma. With the flyer-plate model, such lesions may be further studied on the cellular and subcellular levels. Lasers Surg. Med. 26:364–375, 2000**

Key words: **blast injury; cavitation; endothelial cells; ESWL; Nd-YAG-laser; shock waves**

INTRODUCTION

Several therapeutic procedures involves the generation of shock waves, i.e. excimer laser angioplasty [1], ophthalmologic laser capsulotomy [2,3], laser lithotripsy [4], and extracorporeal shock wave lithotripsy (ESWL) [5]. Pressure transients may also be generated under battlefield conditions, where impact from high velocity missiles and blasts can induce pressure waves within the target [6,7]. Despite this ubiquitous exposure of the human body to high-pressure transients, comparatively little is known about cellular resistance to shock waves and the pathophysiology be-

Contract grant sponsor: Defense Research Establishment.

*Correspondence to: Anders Sondén, MD, Department of Anesthesiology and Intensive Care, Huddinge University Hospital, S-141 86 Huddinge, Sweden.

Accepted 22 October 1999

hind the associated biological damage. Tissue injury associated with ESWL and laser lithotripsy, as well as Nd:YAG-laser capsulotomy, is often attributed to the induction of cavitation [4,8–10]. The destructive mechanisms are assumed to be mechanical, i.e., surface ablation by high-velocity water jet streams generated from collapsing bubbles [11] as well as chemical or thermal, because cavitation generates both reactive oxygen species (ROS) [12] and very high local temperatures [13]. To control simultaneous induction of these collateral effects the flyer-plate model was developed.

Laser radiation has been used for several years to initiate detonation of explosive materials in a highly controlled manner [14–16]. Particularly useful is the indirect approach of laser driven flyer-plates [17,18]. The flyer-plate is generated from a thin layer of metal covering the rear side of a transparent window of fused silica. A high-energy laser pulse aimed at this metal layer through the window will melt and vaporize the inner layers of the metal. The expansion of the hot vapor formed will then accelerate the remaining superficial layer of metal away from the surface as a dish of approximately the same form and size as the laser beam's cross-section. If a target is placed on or in front of this metal sheet (the flyer-plate), part of the kinetic energy will be transformed into a shock wave in the target. This event happens regardless of whether the flyer-plate travels an extremely short [17] or somewhat longer (25–250 μm) distance [18].

The aims of this study were to verify whether the flyer-plate technique was suitable for studying biological shock wave effects on cellular/subcellular levels in vitro and to explore the relevant physical parameters involved. Because detachment of the endothelial layer is one of the characteristic findings in shock wave–induced tissue damage [19–21], we chose to perform the experiments on cultured human umbilical vein endothelial cells (HUVEC).

MATERIAL AND METHODS

Hanks' buffered saline solution without phenol red (HBSS), RPMI 1640 with L-glutamine and phenol red, fetal bovine serum, endothelial cell growth supplement (ECGS, 15 mg/vial), penicillin (10^4 U/ml)-streptomycin (10^4 μg/ml), and Fungizone (Amphotericin B 250 μg/ml) were purchased from Life Technologies (Paisley, United Kingdom). Heparin (5000 IE/ml) was obtained from Lövens Kemiske Fabrik (Ballerup, Denmark). Gelatin (2% solution) was purchased from Sigma Chemicals Co (St. Louis, MO). Catalase type III was from Worthington Biochemical Corporation (Freehold, NJ). Polystyrene 24-well cell culture dishes, Petri dishes (diameter = 35mm) and T-75 cm^2 cell culture flasks were from Nunc (Roskilde, Denmark).

Polyclonal antibodies to coagulation factor FVIII: Rag (vWF), StrAviGen (biotinylated anti-immunoglobulins) and Diluent streptavidin-peroxidase were obtained from Biogenex (Mainz, Germany). The vWF-ELISA kit was from Triolab AB (Mölndal, Sweden). The cell culture incubator was a Steri-cult 200 from Forma Scientific, Inc. (Marietta, OH). LDH was measured spectrophotometrically (Beckman DU-70 Spectrophotometer, Beckman, Fullerton, CA) with a commercially available kit from Boehringer Mannheim (Mannheim, Germany) monitoring NADH formed from NAD+ and lactate. Goat serum was from Dako (Glostrup, Denmark), and hydrogen peroxide was from Merck (Darmstadt, Germany).

The morphometry program used was Bergström Instrument Bildanalys®, Version 1.80, from Bergström Instrument AB (Solna, Sweden). A Nikon Diaphot 300 microscope with a Nikon MD 12 camera (Kodak T MAX® 100 pro, black and white film for paper copies) from Nikon Corp. (Tokyo, Japan) was used for microphotography of cell cultures. Two different YAG-lasers were used, both from Quantel (Paris, France). The laser denoted laser A was a Brilliant B model with an optional beam attenuator module, and the laser denoted laser B was a model YG 581C-10. The energy meter was an Ophir model DGX with a high-energy probe model 30-A-P-RP-DIF from Ophir (Jerusalem, Israel). The laser beam was redirected with a high energy laser mirror bought from Melles Griot (Stockholm, Sweden), type 08MLQ005/426, and was focused with a fused silica symmetric convex lens also from Melles Griot, type 01LQB235. All fused silica windows used as substrate material for vapor deposition of copper were bought from Werner Glas AB (Stockholm, Sweden). The Defense Research Establishment (Stockholm, Sweden) carried out the vapor deposition of copper. The calibrated PVDF pressure transducer with a 1 mm^2 active area came from Ceram (Lund, Sweden). Two types of oscilloscopes were used: oscilloscope A was a HP 54112D (250 M samples/s, Termination 1 MΩ/6.5 pF) bought from Hewlett Packard (Stockholm, Sweden) and oscilloscope B was a Lecroy 7200

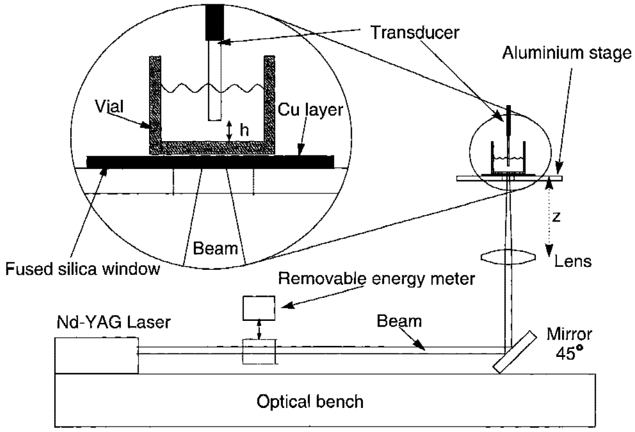

Fig. 1. Schematic illustration of the experimental set-up used when studying physical parameters of the flyer-plate model. During experiments on human umbilical vein endothelial cells, the single vial and the transducer were replaced by 24-well culture plates. Distances in the figure are not proportional to actual set-up; z = variable distance between the lens and the aluminum plate; h = variable distance between the transducer and the inner bottom of the vial (transducer height).

with a plug-in module 7242 (1 G sample/s, Termination 1 MΩ/25 pF) bought from MSS (Åkersberga, Sweden). In one part of the study an optical system consisting of a stereo microscope SMZ-2T from Nikon (Tokyo, Japan), a CCD Iris Color Video Camera SSC-C370P bought from Sony (Stockholm, Sweden), and a monitor LDH 2106/00 from Phillips (Eindhoven, The Netherlands), was used. Sequential photography was conducted with a Nikon ESR camera with a Kodak Ektapress® Gold 400 color film for paper copies together with a Druello xenon flash and a DG 535 delay and pulse generator from Stanford Research Systems Inc. (Sunnyvale, CA). A fast photo diode pin detector system, model 875, from Newport (Fountain Valley, CA) was used to verify the duration of the xenon flash output.

The Flyer-Plate Model

A schematic representation of the experimental set-up used is shown in Figure 1. Two lasers, both with a wavelength of 1,064 nm, were used in different phases of the study. Laser A had a pulse width of about 5.5 ns, whereas laser B had a broader pulse width of about 12 ns. Laser A was used in a majority of the experiments, including the entire cell culture exposures. The output energy from laser A was altered with the use of the built in beam-attenuator module. Before each individual experiment the energy level was set and controlled with at least five single firings. The level was verified in the same way after the experiment. The spread and the time drift of the laser energy level were never greater than 5%.

A coated high-energy mirror, a focusing lens (focal length 250 mm), and an aluminum stage with a circular (diameter = 10 mm) aperture were mounted in holders on a vertical stand on a horizontal optical bench. The alignment of the components ensured that the laser beam reached the 1.5-mm-thick circular (diameter = 32 mm) fused silica window, with a 7-μm-thick layer of copper vapor deposit on the top side, placed on the aluminum stage, and covering the aperture. The cell culture vial was placed on top of the fused silica window in immediate contact with the copper layer and, thus, was subjected to the impact of the accelerating flyer-plate. The distance between the lens and the aluminum plate (z) could be varied to some extent by means of a micrometer screw without altering the overall alignment. The laser beam cross-section on the target, measured from imprints on light sensitive paper, was elliptical with a major axis of approximately 3.2 mm and a minor axis of approximately 2.7 mm for z = 19.7 cm (the distance used in the majority of the experiments).

The vial mainly used for the measurements of the physical parameters (vial A) was a single well cut out from a 24-well cell culture plate. For comparison, a Petri dish (vial B) was used in some of the experiments. In experiments on HUVECs, 24-well cell culture plates were used. Vial A and the 24-well plates were always used together with laser A, and vial B always together with laser B. In the test series, the vial was filled with tap water at room temperature, pH 6.8–7.2.

Shock wave pressure as a function of time and the time of arrival of the shock wave front (t_{start}) were registered, at several locations in the vial water, with a PVDF pressure transducer. The transducer was connected either to oscilloscope A (laser A, vial A) or to oscilloscope B (laser B, vial B), always with the highest possible temporal resolution. Time was measured in relation to the onset of the laser pulse. At this instant, the laser control unit also triggered the oscilloscope. The distance between the transducer and the inner bottom of the vial (transducer height [h]) could be varied by means of micrometer screws. The transducer was always aligned with the laser beam, thereby, also with the impact area of the flyer-plate.

The peak pressure of the shock wave (p_{peak}),

t_{start}, the half width of the first pressure peak, and the tailing negative (tension) part of the shock wave registration were obtained at different transducer heights for a total of 128 firings at both types of vials. The experiments were divided into two test series that used two fused silica plates for each type of vial. Transducer heights used in vial A were 0.5, 1.0, 2.0, 4.0, and 8.0 mm. Corresponding heights in vial B were 0.5, 1.0, 1.5, 3.0, 4.0, and 7.5 mm. In these test series, the water column height always exceeded 10 mm.

The sensitivity to variations in the laser energy (0.29, 0.56, or 0.70 J) or the distance z (18.9, 19.7, or 20.3 cm) of p_{peak} and t_{start} was measured in vial A together with laser A. The transducer height was 0.9 mm. One fused silica plate was used for the laser energy variation test series and another for test series of the variation of distance z. Total number of firings was 43. To compare the results statistically for both types of variations a null hypothesis was postulated, that each three mean values of either the peak pressure or the time of arrival of the shock front were the same. As test criterion, the relation between the individual calculated 99% confidence intervals, assuming a normal distribution, was used. If the confidence intervals were not overlapping, the null hypothesis was rejected with a significance ($P < 0.01$), corresponding to the level of the confidence intervals.

The response of the water in the vial to the impact of the flyer-plate was studied as follows: (1) In connection with flyer-plate impact bubble formation and ejection of droplets from the water surface was observed. The threshold, expressed as a probability function of water volume (liquid column height), for the onset of this observation, believed to be caused by cavitation, was estimated with a modified up-and-down approach [22]; a test approach commonly used to connect a continuous probability function of a chosen variable to the occurrence of a digital phenomenon i.e. a "go/no-go" phenomenon. In vial A, four volumes (0.3, 0.6, 0.9, and 1.2 ml) were used with 8 impacts/volume, whereas in vial B, six volumes (2.0, 2.5, 3.0, 3.5, 4.0, and 4.5 ml) with 12 impacts/volume were used. The test approach was modified in the sense that all firings at a certain water volume were made in an uninterrupted sequence. The occurrence of cavitation in the water was detected with the naked eye and on the video monitor attached to the stereo microscope, magnification ×4. In addition a transparent lid was placed on top of the vial to register any ejection of liquid from the vial. The number of "gos" (occurrence of cavitation) and "no-gos" were counted. By using the computer code ML-14 [23], a normal distribution was fitted to the data and probability levels (with confidence intervals) for the occurrence of cavitation was calculated as a function of water volume and as a function of water column height. The volumes corresponding to a 50% probability and a 0.01% probability for the occurrence of cavitation, thus, were determined. Volumes used during the sequential photography and experiments on HUVECs *(vide infra)* were based on these results. (2) The sensitivity of the naked eye observations was estimated by comparison with a time sequence of pictures of vial A after flyer-plate impact, obtained in the following manner: By darkening the laboratory and by using a camera with an open aperture together with a fast xenon flash (nominal duration 1 μs) connected to a trig and delay unit, it was possible to take pictures of the vial at different times after the flyer-plate impact. The trig and delay unit was trigged from the laser control unit at the onset of the laser pulse. Delay times set were 5, 20, and 500 μs. The light from the xenon flash peaked after about 450 ns. The width at half the maximum light level was about 640 ns. Values were controlled with a photo diode and an oscilloscope before the actual experiment. Water volumes used were either 0.6 or 2.4 ml.

Cell Culture Technique

Human umbilical cords were obtained after normal deliveries, kept sterile, and treated with 0.2% collagenase to harvest venous endothelial cells as previously described [24,25]. Cells from at least two umbilical cords were pooled, resuspended in cell culture medium (RPMI 1640 with 20% calf serum, heparin 90 g/ml, penicillin 100 U/ml, streptomycin 100 U/ml, amphotericin B 0.25 μ g/ml and ECGS 50 μg/ml) and seeded in T 75 cm^2 cell culture flasks precoated with 0.2% gelatin. The culture medium was changed the following day and thereafter twice a week. When confluent, cultures were trypsinized, subcultured in 24-well cell culture dishes precoated with 0.2% gelatin and maintained in a 5% CO_2/95% humidified air atmosphere at 37°C. Confluent cultures from passage 2–3 were used for experiments. Cells were characterized by their cobblestone appearance in the phase contrast microscope and immunocytochemical staining for vWF (FVIII: Rag).

Phase Contrast Microscopy and Computerized Morphometry

The vials of a 24-well cell culture dish with HUVECs were filled with either 2.4 ml or 0.6 ml HBSS with 1% BSA. Each vial was positioned above the fused silica window and submitted to a single shock wave generated by the flyer-plate, by using laser A (output energy 0.6 J, z = 19.7 cm). Vials containing 0.6 ml, for which no bubble formation and ejection of liquid were registered, were excluded from the experiments. After exposure, the buffer was collected and frozen at –70°C until analyzed. One set of cells was washed twice, fixed in 2% formaldehyde in HBSS, and stained with hematoxylin and eosin to examine general morphology. Another set was stained in situ with 0.2% Trypan blue in HBSS, to assess cell membrane damage. After additional washings, cells were mounted in their wells with glycerine-gelatin, examined under phase contrast microscopy, and photographed by using automatic exposure times. Thereafter, the cell culture vials (n = 24) were coded. Microscopic images were processed with a computerized morphometry program. The areas of interest were manually selected and marked, and their surface areas were measured.

Analysis of vWF (FVIII: Rag) and LD

After washings, confluent HUVEC monolayers covered with either 2.4 ml or 0.6 ml of HBSS supplemented with 1% BSA were submitted to a shock wave. Again, the 0.6-ml vials for which no bubble formation and ejection of liquid were registered, were excluded. After exposure, the vials were placed in an incubator at 37°C for 0, 1, 4, and 16 hours. At indicated time intervals, buffer from each well was collected and stored at –70°C until analyzed for vWF (n = 96) or LD (at 4 hours exclusively) (n = 15) by using enzyme-linked immunosorbent assay or spectrophotometry, respectively. Cultures were then washed and fixed in 95% ethanol, washed again, and incubated in 3% H_2O_2 to avoid background staining. After additional washing, cells were incubated with 10% bovine serum in HBSS before they were incubated with monoclonal antibodies to vWF overnight at 4°C in a humidified incubation chamber. The following day, cells were incubated with secondary antibodies for 30 minutes, washed, and incubated with HRP-conjugated streptavidin for another 30 minutes. Finally, cultures were incubated with DAB, washed with distilled water, and mounted in their wells with glycerine-gelatin. The cultures were examined under phase contrast microscopy and photographed. All incubations, except when said otherwise, were performed at room temperature. The Wilcoxon rank sum test was used for statistical inference of endothelial lesion areas, and vWF and LD release to the medium. Statistical significance was considered at P values < 0.05.

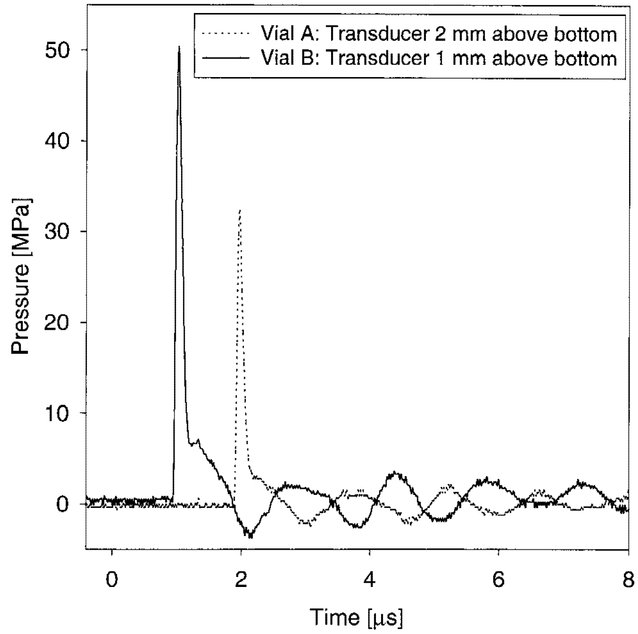

Fig. 2. Representative transducer signals generated by flyer-plate impact on the exterior bottom surface of a single vial. The dotted curve was registered in vial type A with the transducer at h = 2 mm and the solid line in vial type B with the transducer at h = 1 mm. h = variable distance between the transducer and the inner bottom of the vial (transducer height).

RESULTS

Characteristics of the Shock Wave and Related Phenomena

The flyer-plate impact resulted in a small elliptical opaque area on the external bottom surface of the vial. The extension of this area (major axis of about 1.6 mm and minor axis of approximately 1.0 mm) was slightly smaller than that of the corresponding hole in the copper layer on the fused silica plate.

Typical transducer signals induced by flyer-plate impact in vial A and vial B are shown in Figure 2. The mean peak pressure as a function of transducer height is shown in Figure 3 for both types of vials. Each individual point in the dia-

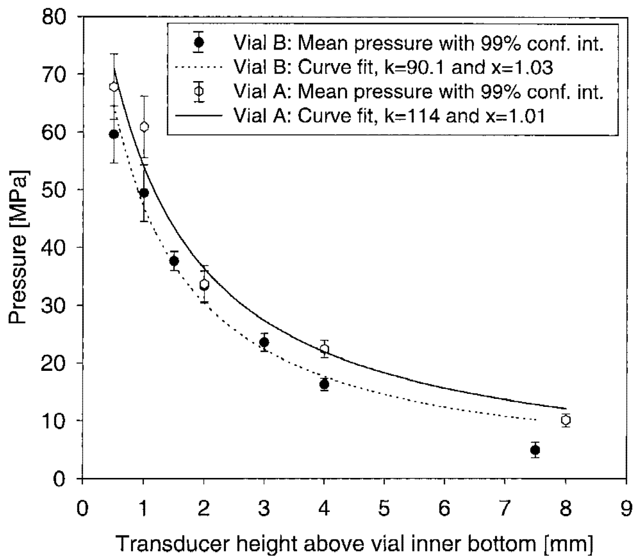

Fig. 3. Mean peak pressure measured with the transducer, as a function of distance above the interior vial bottom surface, h. Open hexagons represent mean values obtained in vial type A, and the black circles represent mean values from vial type B (n = 5–19). Error bars represent 99% confidence intervals assuming a normal distribution are also shown. The solid and the dotted curve are the results from nonlinear regressions to fit individual peak pressure values from each type of vial to a function $p = k/r^x$, where p is the peak pressure, r = h+ (thickness of vial bottom), and k and x are parameters varied to find the best fit.

gram is a mean value of between 5 and 19 firings for which each individual silica window could be used for approximately 40 firings. Maximal mean peak pressures in vial A and vial B reached at h = 0.5 mm were 67 MPa and 60 MPa, respectively.

Because the amplitude of the negative part of the pressure signal was only a small fraction of the total amplitude range, the resolution in measuring the negative peak value was poor. It was possible, however, to discern that the first negative peak was always the deepest and that its maximal negative value decreased with increased transducer height: from 6 MPa at h = 0.5 mm down to 3 MPa at h = 8 mm in vial A, and from 4 MPa at h = 0.5 mm down to 1 MPa at h = 7.5 mm in vial B. The frequency of the always-present damped oscillation in the tail of the pressure signal was about 700 kHz.

The mean half-width of the first positive peak was ≅ 145 ns (standard deviation [σ] = 17 ns) in vial A for h between 0.5 and 2 mm and ≅ 120 ns (σ = 9 ns) in vial B for h between 0.5 and 4 mm increasing to ≅ 175 ns (σ = 9 ns) in vial A for h = 4 mm and h = 8 mm and to ≅ 155 ns (σ = 21 ns) in vial B at h = 7.5 mm. By using a simple linear regression on the mean values of t_{start} as a function of transducer height, the mean shock front velocity was calculated to 1.5×10^3 m/s for both vials.

The sensitivity of the peak pressure and the time of arrival of the shock wave front to variations in the laser energy and in the distance z was measured. Between the two highest energy levels (0.56 J and 0.73 J) there were no statistically significant differences, regarding neither the peak pressure (59.3 ± 3.0 MPa vs. 61.4 ± 3.9 Mpa) nor the time of arrival of the shock front (1,054 ± 23 ns vs. 1,070 ± 16 ns). However, a slight but significant ($P < 0.01$) decrease in peak pressure (39.1 ± 1.5 MPa) and a corresponding increase in time of arrival (1,112 ± 11 ns) were seen when the laser output energy was lowered to 0.29 J. The variation of the distance z did not reveal any statistically significant differences neither in peak pressure nor in time of arrival of the shock front. Results from the up-and-down tests are shown in Table 1. The results are expressed as the volume (water column height) corresponding to a 50% probability and a 0.01% probability for the occurrence of bubble formation and ejection of water. Hence, the probability of this observation in vial A was shown to be less than 0.01% when the vials were filled with 2.4 ml of water and greater than 50% when the vials were filled with 0.6 ml.

Thus, in vials containing 0.6 ml, cavitation was detected with the naked eye and on the monitor in connection with the flyer-plate impact. The observation commenced with the formation of tiny bubbles adjacent to the water surface in alignment with the impact area. Subsequently, the bubbles moved from the area of generation both parallel with the surface and toward the bottom. In addition, at about the same instant as the bubble formation, one or a few droplets of water were ejected from the surface and caught on the transparent lid covering the vial. In vials containing 2.4 ml, the phenomenon was never observed.

From the time sequence of pictures of vial A, filled with either 0.6 ml or 2.4 ml of water, the following observations were made: at 5 μs, with respect to the onset of the laser pulse, bubbles were seen adjacent to the surface in the 0.6-ml vial. Additional bubble formation not observed with the naked eye or on the monitor was detected at the bottom of both vials. After 20 μs, the bubbles at the bottom were larger in both vials. Concomitantly, the bubbles at the top bulged above the surface in the 0.6-ml vials (Fig. 4a,b). At 500 μs, the bubbles at the bottom had disap-

TABLE 1. Results from Up-and-Down Measurements Showing Both the 50% Probability Level and the 0.01% Probability Level for the Occurrence of Cavitation in Tap Water

Type of vial	50% Probability level[a]	0.01% Probability level
Vial A (32 shots)	0.71 ml (0.57–0.83 ml) (3.9 mm [3.1–4.7 mm])[b]	1.3 ml (1.0–4.5 ml) (7.0 mm [5.7–13 mm])[b]
Vial B (65 shots)	3.4 ml (3.2–3.6 ml) (3.8 mm [3.6–4.0])[b]	4.7 ml (4.2–5.8 ml) (5.2 mm [4.7–6.5 mm])[b]

[a]With 95% confidence intervals.
[b]Corresponding surface height, calculated neglecting surface tension.

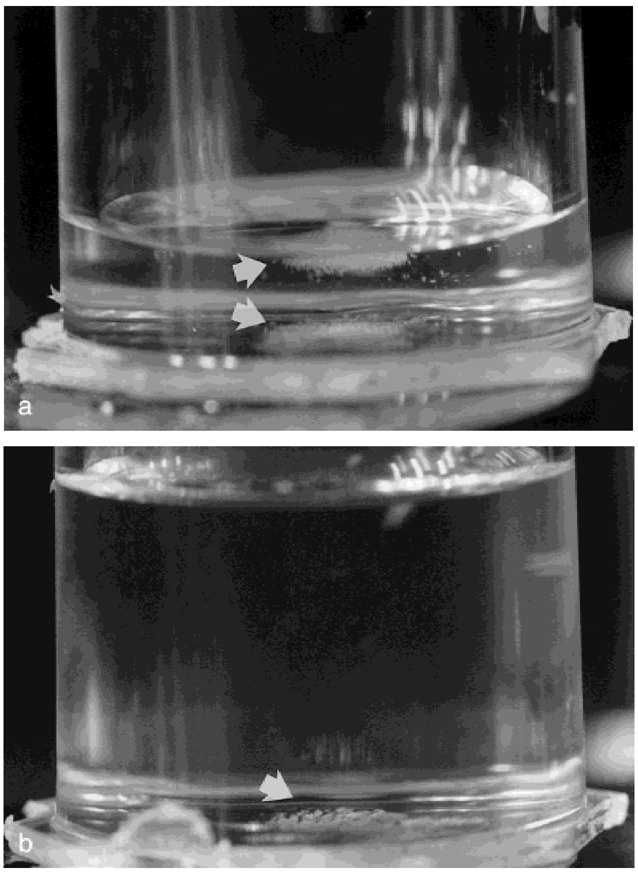

Fig. 4. Examples from the sequence of photographs of a cell culture vial at different delay times with respect to the flyer-plate impact. **a:** A vial with 0.6 ml of water 20 μs after impact. Bubble formation (cavitation) is seen adjacent to the water surface and at the bottom of the vial (arrows). **b:** The same vial at the same delay time but now filled with 2.4 ml of water. Here, bubble formation (cavitation) is seen at the bottom exclusively (arrow).

peared in both vials. Ejection of water was seen in the 0.6-ml vial reaching 4–5 mm above the surface. When compared with sequential photography the sensitivity for the detection of cavitation at the surface with the naked eye or by means of droplets caught on the transparent lid was 100%.

Shock Wave Effects on HUVECs

Within less than 5 minutes after flyer-plate impact, a limited area with cell injury covering and adjacent to the impact mark could be distinguished from the surrounding culture in the phase contrast microscope. The demarcation between this area and the surrounding culture is shown in Figure 5.

When measured with computerized morphometry, the injured area was found to be significantly larger in vials containing 0.6 ml of buffer, i.e., in vials for which cavitation had been induced at the bottom and at the surface. Lesion area (mean ± SEM) in the 0.6-ml vials was 8.01 ± 1.2 mm^2 vs. 6.4 ± 1.9 mm^2 in the 2.4-ml vials ($P <$ 0.01).

Release of LD (mean ± SEM) to the culture medium was significantly elevated ($P < 0.01$) in wells submitted to a shock wave compared with controls with numerical values of 4.8 ± 0.5 U/ml in the 0.6-ml vials, 4.7 ± 0.7 U/ml in the 2.4-ml vials and 3.4 ± 0.6 U/ml in control vials. No statistically significant differences between the 0.6- and the 2.4-ml vials, however, could be demonstrated.

In hematoxylin-eosin stained samples, rupture of cell membranes and large amounts of cell debris within the endothelial lesion was demonstrated together with condensed, pyknotic cell nuclei with prominent nucleoli. Numerous cells had detached from their substratum (Fig. 6a). No morphologic differences were found between cells peripheral to the endothelial lesion and controls not subjected to the flyer-plate impact.

When cell membrane integrity was examined in situ with trypan blue, cells within the lesions exhibited a weak diffuse staining. Cells peripheral to the lesion and control cultures completely failed to take up the dye. Finally, cell-bound expression of vWF did not differ between exposed HUVECs and controls, nor did the vWF-release to the media when measured 15 min, 1, 4 and 16 hours after exposure.

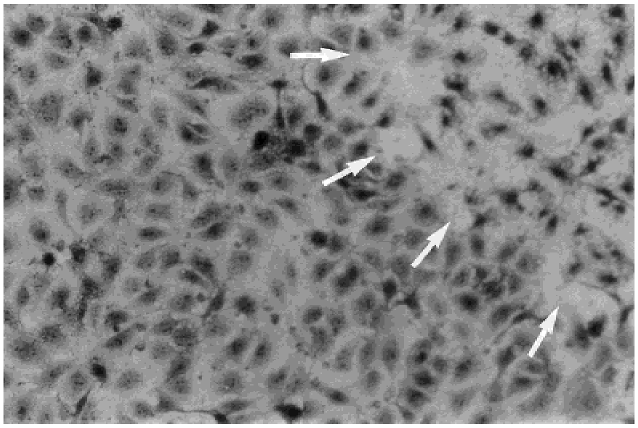

Fig. 5. Photomicrograph of a human umbilical vein endothelial cell culture after flyer-plate impact. The picture illustrates the demarcation zone (arrows) between apparently unaffected (left) and damaged cells (right). Hematoxylin-eosin stain. Original magnification, ×50.

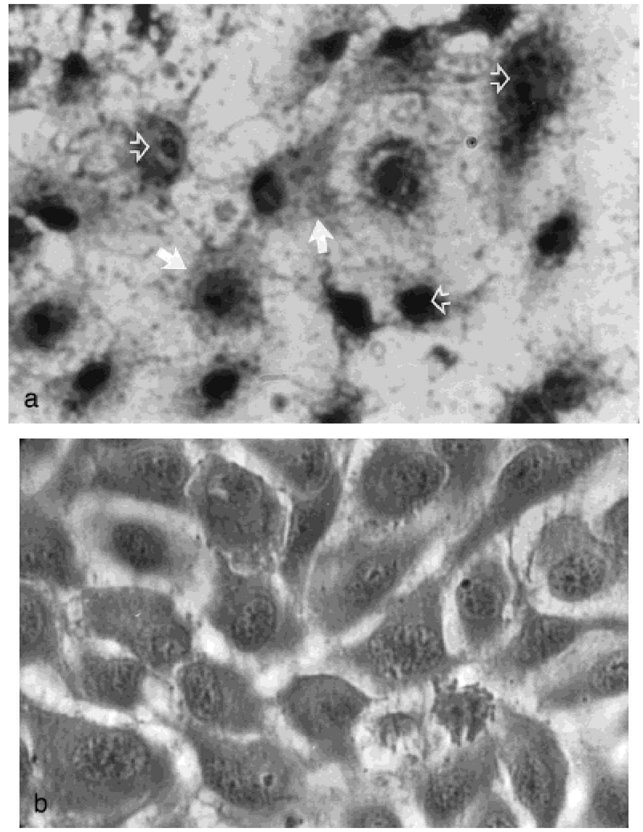

Fig. 6. **a:** Photomicrograph illustrating cell injury induced by the shock wave and concomitant cavitation. Condensed, pyknotic cell nuclei with prominent nucleoli are seen (open arrows). Cell borders are difficult to define (filled arrows) and large amounts of cell debris are spread throughout the lesion area, indicating rupture of the cell membranes. Original magnification ×100. **b:** Photomicrograph of a normal human umbilical vein endothelial cells (HUVEC) culture. Hematoxylin-eosin stain Original magnification, ×100.

DISCUSSION

The Shock Wave

The shock wave was highly reproducible (Figs. 2, 3). The first positive (compressive) peak had a high amplitude, p_{peak}, a very fast rise time, and was followed by a negative (tension) pressure peak. Unfortunately, p_{peak} could not be measured directly at the inner bottom of the vial (h = 0), because the transducer was permanently damaged in trying to do so. Instead, the value of p_{peak} at h = 0 was extrapolated from measurements of p_{peak} at other distances above the inner bottom. Therefore, the measured p_{peak} values were fitted to equation (1) below, by means of nonlinear regression.

$$p_{peak} = \frac{k}{r^x} \tag{1}$$

In equation (1), r is the distance from the impact and, hence, r = h + (thickness of vial bottom) and k and x are the parameters varied to find the best fit. The resulting curves are plotted in Figure 3, where the corresponding parameter values can also be found. With this equation p_{peak} at h = 0 was calculated to 104 MPa in vial A and to 10^3 MPa in vial B.

The shock wave velocity, 1.5×10^3 m/s is in good agreement with the velocity of sound in water at room temperature, 1.497×10^3 m/s [26]. However, if only the difference in t_{start} between h = 0.5 mm and h = 1.0 mm is used the mean shock wave velocity becomes 1.7×10^3 m/s in vial A and 1.8×10^3 m/s in vial B. This together with the obvious deviation from the 1/r-curve for p_{peak}, measured at h = 8 mm and h = 7.5 mm in vial A and vial B, indicates an incoming shock wave with gradually decreasing peak amplitude eventually becoming a sound wave. If a wave is propagating spherically or hemispherically out from a point source, its amplitude is inversely proportional to the distance, r, from the source [2,27]. For a strong shock wave, the decay of the amplitude is faster than 1/r due to the strong dissipation of energy into heat at the shock front [2,27]. However, in the flyer-plate model, the maximal shock wave pressure is only moderate and the decay should not deviate much from 1/r, as seen in Figure 3. Furthermore, the shock-generating source is flat and a hemispherical propagation cannot be assumed, at least not until rarefaction waves from the impact boundary can catch up with the

main compression wave [28]. This, however, seems to have happened at the lowest transducer height used, h = 0.5 mm.

Cavitation at the Vial Bottom

The bubble formation detected at the bottom of the vials with sequential photography (Fig. 4) is assumed to be cavitation, i.e., the rupture of the liquid-solid (water-inner vial bottom) interface, due to reduction of the local static pressure caused by a rarefaction wave emanating from the release of the compressive forces of the flyer plate on the exterior vial bottom. The first negative peak in (Fig. 2) is probably a representation of this rarefaction wave. According to the manufacturer, the transducer is also, at least to some extent, linear in its response to negative pressure (tension), but has a resonant frequency at about 700 kHz. Therefore, the source of the oscillations after the first negative peak is unclear and could possibly be the transducer itself.

Cavitation is usually located at a boundary between different materials [29], it does not occur until a threshold is reached [30], and the threshold increases as the duration of the tension decreases [29,31]. For tension wave duration of 500 μs, the threshold value for tap water has been demonstrated to be 0.9 MPa [32–34]. In the flyer-plate model, tension duration is much shorter, but the negative peak value is much higher.

The duration of the cavitation at the bottom of the vial (bottom cavitation) was too short to enable detection with naked eye observations or by a video framing speed of 25 Hz. However, when photographed, bottom cavitation was always present and did not depend on water volumes used. Therefore, it is assumed that with the flyer plate model the tension induced at the water-vial bottom interface is well above the threshold and that bottom cavitation is always generated after the flyer-plate impact. Because only minor adjustments are possible in the shock wave generation of the model, no evaluation of the actual threshold was carried out.

Cavitation at the Surface

In the case of surface cavitation, the drop in local pressure is caused by the pressure release at the liquid-air interface as the shock wave arrives. When the results in Table 1 (both types of vials) are compared, it is obvious that the occurrence of surface cavitation depends on liquid column height rather than on liquid volume. Because p_{peak} decreases with increasing h, it is also very possible that the peak pressure is an important parameter.

To describe the resistance to cavitation, a parameter without dimension, i.e., the cavitation number, κ, can be defined [29,30] as the ratio of the difference between the ambient static pressure, p_0, and the vapor pressure, p_v, and the dynamic pressure of a flow.

$$\kappa = \frac{p_0 - p_v}{\frac{1}{2}\rho_0 u_p^2} \tag{2}$$

In equation (2), ρ_0 is the uncompressed liquid density and u_p the liquid flow velocity. The higher the cavitation number, the less likely cavitation is to occur, and vice versa. To mark the threshold between occurrence of cavitation and not, the critical cavitation number, κ_{crit}, can be introduced [32,33].

As the shock wave propagates through the water in the vial, a local flow of the liquid is induced, i.e., the particle velocity. From simple one-dimensional theory of shock waves (e.g., Ref. 26) the following three useful relations can be obtained.

$$p - p_0 = \rho_0 U_s u_p \tag{3}$$

$$v_{fs} = 2u_p \tag{4}$$

$$\frac{\rho}{\rho_0} = \frac{U_s}{U_s - u_p} \tag{5}$$

In equations (3), (4), and (5), p is the amplitude of the shock wave, i.e., dynamic pressure, U_s the wave velocity, u_p the particle velocity, v_{fs} the free surface velocity, and ρ the shock-compressed density.

According to Ross [29] the critical cavitation number for a flow situation, where the flow velocity changes abruptly from u_0 to u_1, can be calculated as follows in equation (6).

$$|\kappa_{crit}| = \left(\frac{u_1}{u_0}\right)^2 - 1 \tag{6}$$

The upper water surface in the vial can be seen as a free surface, and, hence, equation (4) can be inserted into equation (6) and a critical cavitation number of 3.0 results. By using equations (3) and (2), the threshold (minimum) peak

pressure amplitude, p_{crit}, resulting in surface cavitation can be calculated.

$$p_{crit} = U_s\sqrt{\frac{(p_0 - p_v)2\rho_0}{\kappa_{crit}}} - p_0. \quad (7)$$

Doing so with the following parameters, $U_s = 1.5 \times 10^3$ m/s (wave velocity), $\rho_0 = 998$ kg/m^3, $p_0 = 1$ atm $= 0.101$ MPa, and $p_v = 2.33$ kPa results in $p_{crit} = 12$ MPa.

Equations (2) and (6) are both deduced from Bernoulli's equation and, therefore, anticipating an incompressible flow. By using equation (5), the degree of compression at p_{crit} is calculated to be only 0.4%; thus, the assumption of incompressible flow seems to be a reasonably good approximation.

By using equation (1), the corresponding critical liquid column height for vial A was calculated to 8.0 mm (1.5 ml) and for vial B to 6.1 mm (5.5 ml). If compared with the values in Table 1 for 0.01% probability of surface cavitation, the critical liquid column height is well inside the 95% confidence interval for both vials. So, even if equation (7) does not take into consideration any possible capacity of the water to withstand at least some tension, the equation can be used to explain the experimental observations and, hence, to predict the occurrence of surface cavitation with, for the flyer-plate method, good enough accuracy.

Of minor interest, but still of some importance, is the observation of the excellent stability of the peak pressure amplitude to variations in laser energy and in focal distance. Influence from time drift in the laser output energy and from small misalignments, therefore, was negligible.

Biological Relevance

Shock wave-induced tissue injury is a frequently reported phenomenon with clinical importance in vascular surgery, ophthalmology, urology, and traumatology. In pulsed laser angioplasty, shock waves play an important role in tissue ablation [35] but are, on the other hand, considered to be responsible for adjacent tissue damage [1]. Shock waves generated during ESWL are known to cause side effects such as transient hematuria and sometimes subcapsular renal hematomas [36]. In experimental ESWL models, shock waves have been shown to induce defined areas with endothelial denudement of the basement membrane and extravasation of red blood cells, principally within the microvasculature of the kidney [19,21], probably explaining the transient hematuria. Similar lesions have been seen in the corneal endothelium after Nd:YAG laser surgery [10,37] and in the major vessels of Atlantic salmon when studying the effects of underwater explosions [38]. Little is known about the pathophysiology causing shock wave associated biological damage, why more sophisticated models for the study of shock wave-cell interactions are warranted.

With the flyer-plate model, we provide an experimental arrangement in which monolayers of any cell type may be exposed to a defined, reproducible shock wave. Because vascular injury is frequently reported in association with shock wave exposure [19,21,39], we used HUVEC in our experiments. The shock wave generated induced cavitation in the cell culture vials, either at the bottom solely or at the bottom and the surface depending on the prechosen height of the fluid column. Thus, the extent of cavitation could be varied and determined in advance for each cell culture vial.

We demonstrated that one shock wave, in combination with cavitation, caused endothelial cell membrane damage, cell detachment, and subsequently death of endothelial cells. The cell injury was limited, defined, and reproducible, and was significantly larger in vials where the monolayers were exposed to the higher extent of cavitation. When processing the cultures further (e.g., rinsing), injured cells detached from the substratum, creating a defined denuded area. The resemblance to in vivo lesions [10,19,37,38] is persuasive and suggests a similar pathophysiologic process. The inability to visualize the primary effect on the endothelial cell membrane in the in vivo experiments [10,19,37,38] may be caused by rinsing during tissue fixation, because this would most likely detach injured cells. Therefore, we suggest that our in vitro results also account for the in vivo situation.

The physical mechanisms underlying shock wave–induced tissue and vessel damage are complex and not fully understood. Direct mechanical forces and the induction of cavitation have to be considered [11]. The propagation of the pressure transient causes acceleration and displacement of particles/cells. The compressive and tensile forces are particularly pronounced at interfaces between materials with different acoustic impedance, i.e., blood-endothelium and/or alveolar epithelium-air [38]. Several ESWL studies confirm that cellular

damage in vivo preferentially occurs at such interfaces [20,39]. The issue is complicated by the fact that cavitation can be induced in any liquid within the body, where the tensile forces exceed the tensile strength of the fluid, which will be at the same interfaces. Cavitation has indeed been demonstrated during ESWL and laser lithotripsy as well as Nd:YAG laser capsulotomy and is thought to contribute to the associated tissue damage [2,4,8]. The collapsing cavitation bubbles creates liquid jets and secondary shock waves, which may cause severe damage to nearby boundary surfaces [4,11]. Furthermore, cavitation has been showed to generate ROS and extreme temperatures, which can cause additional tissue injury [12,13]. Considering that the characteristic appearance of the endothelial injury does not seem to be affected by differences in pressure wave amplitude, duration, frequency, or total number of shock waves applied [19,20,33] a governing, common destructive mechanism causing the endothelial damage is suggested, possibly cavitation. Our results with the flyer-plate model suggest a dose-response relationship between the extent of cavitation and cellular injury. Differentiation of the physical mechanisms involved in shock wave induced tissue injury would be of major interest and may even have future clinical implications.

CONCLUSION

To conclude, we have demonstrated that the flyer-plate model can be used to subject cell monolayers to accurate and reproducible compressive shock wave transients. Cells within a limited area were constantly submitted to simultaneous bottom cavitation, whereas surface cavitation could be “turned on or off” by adjusting the height of the liquid column in the wells. The inflicted cell injury was immediate, defined, and presumably caused by cavitation interacting with the cell membrane. The resemblance to the previously described endothelial lesions associated with ESWL, Nd:YAG laser capsulotomy, and blast trauma suggests a similar pathophysiologic process. With the flyer-plate model, such lesions may be further studied on the cellular and subcellular levels.

ACKNOWLEDGMENTS

The authors thank E. Malm, I.-L. Larsson, S. Björklund, and C. Forsbom for excellent technical assistance, K. Ormegaard for his photographic expertise, and Dr. H. Almström and H. Axelsson for valuable discussions concerning shock waves and cavitation.

REFERENCES

1. Haase KK, Rose C, Duda S, Baumbach A, Oberhoff M, Anthanasiadis A, Karch KR. Perspectives of coronary excimer laser angioplasty: multiplexing, saline flushing, and acoustic ablation control. Laser Surg Med 1997;21: 72–78.
2. Vogel A, Hentschel W, Holzfuss J, Lauterborn W. Cavitation bubble dynamics and acoustic transient generation in ocular surgery with pulsed neodymium-YAG lasers. Ann Ophthalmol 1986;93:1259–1269.
3. Juhasz T, Kastis GA, Suáres C, Bor Z, Bron BE. Time resolved observations of shock waves and cavitation bubbles generated by femtosecond laser pulses in corneal tissue and water Laser Surg Med 1996;19:23–31.
4. Rink K, Delacrétaz G, Salathé R. Fragmentation process of current laser lithotriptors. Laser Surg Med 1995;16: 134–146.
5. Brendel W, Chaussy CH, Forsman B, Schmiedt E. A new method of noninvasive destruction of renal calculi by shock waves. Br J Surg 1979;66:907.
6. Suneson A, Hansson H-A, Seeman T. Peripheral high-energy missile hits cause pressure changes and damage to the nervous system: experimental studies on pigs J Trauma 1987;27:782–789.
7. Clemedsson CJ. Blast injury. Acta Physiol Scand 1956;6: 336–354.
8. Fisher N, Muller HM, Gulhan A, Sohn M, Deutz FJ, Rubben H, Lutzeye W. Cavitation effects: possible cause of tissue injury during extracorporeal shock wave lithotripsy. J Endourol 1988;2:215–220.
9. Delacrétaz G, Rink K, Pittomvils G, Lafaut JP, Vandeursen H, Boving R. Importance of the implosion of ESWL-induced cavitation. Ultrasound Med Biol 1995;21: 97–103.
10. Martin NF, Gaasterland DE, Rodrigues MR, Thomas G, Cummins CE. Endothelial damage threshold for retrocorneal Q-switched neodymium-YAG laser pulses in monkeys. Opthalmol 1985;92:1382–1386.
11. Coleman AJ, Saunders JE, Crum LA. Dyson M. Acoustic cavitation generated by an extracorporal shockwave lithotripter. Ultrasound Med Biol 1987;13:69–76.
12. Suhr D, Brummer F, Irmer U, Schlachter M, Holser DF. Reduced cavitation-induced cellular damage by the antioxidative effect of vitamin E. Ultrasonics 1994;32:301–307.
13. Crum LA, Roy RA Sonoluminescence. Science 1994;220: 233–234.
14. Brish AA, Galeeva IA, Zaitsev BN, Sbitnev EA, Tatarinstev LV. Mechanism of initiation of condensed explosives by laser radiation. Fizika Gorenyia i Vzryva 1969;5:475–480.
15. Yang LC, Menichelli VC. Detonation of insensitive high explosives by a Q-switched Ruby laser. Appl Phys Lett 1971;19:473–475.
16. Paisley DL. Prompt detonation of secondary explosives by a laser. In: Proceedings of the Ninth Symposium (International) on Detonation, August 28–September 1, Portland, Oregon, 1989. p 1110–1117.

17. Yang LC. Stress waves generated in thin metallic films by a Q-switched Ruby laser. J Appl Phys 1974;45:2601–2608.
18. Paisley DL. Laser-driven miniature flyer plates for shock initiation of secondary explosives. In: Schmidt SC, Johnson JN, Davison LW, editors. Shock compression of condensed matter-1989. Amsterdam: Elsevier Science Publishers BV; 1990. p 733.
19. Brendel W, Delius M, Goetz A. Effects of shock waves on the microvasculature. Prog Appl Microcirc 1987;12:41–50.
20. Steinbach P, Hofstaedter F, Nicolai H, Roessler W, Wieland W. Determination of energy-dependent extent of vascular damage caused by high-energy shock waves in an umbilical cord model. Urol Res 1993;21:279–282.
21. Seidl M, Steinbach P, Wörle K, Hofstädter F. Induction of stress fibers and intercellular gaps in human vascular endothelium by shock waves. Ultrasonics 1994;32:397–400.
22. Dixon WJ, Masey FJ. Introduction to statistical analysis. New York: McGraw-Hill; 1957. p 318–327.
23. Johansson H. ML14: a computer program to calculate the parameters in a standard distribution and the levels of confidence, Swedish Defense Research Establishment, FOA report no. C20748-23, 1989.
24. Jaffe EA, Nachman RL, Becker CG, Miniek R. Culture of human endothelial cells derived from umbilical veins. J Clin Invest 1973;52:2745–2756.
25. Lerner R, Lindström P, Palmblad JP. Platelet activation factor and leukotriene B induce hyperpolarization of human endothelial cells but depolarization of neutrofils. Biochem Biophys Res Commun 1988;153:805–810.
26. Cooper PW, Kurowski SR. Introduction to the technology of explosives. New York: VCH Publishers Inc; 1996. p 57–82.
27. Cole RH. Underwater explosions. Princeton: Princeton University Press; 1948. p 5–13.
28. Nicholas T, Recht RF. Introduction to impact phenomena. In: Zukas JA, editor. High velocity impact dynamics. New York: John Wiley & Sons, Inc; 1990. p 1–65.
29. Ross D. Mechanics of underwater noise. New York: Pergamon Press; 1976. p 202–252.
30. Young FR. Cavitation. London: McGraw-Hill; 1989. p 4, 190, 248.
31. Urick RJ. Principles of underwater sound. 3rd ed. New York: McGraw-Hill Book Company, Inc; 1983. p 77–81.
32. Trevena DH. The liquid phase. London: Wykeham Publications, Ltd; 1975. p 70.
33. Trevena DH. Cavitation and the generation of tension in liquids. J Phys D Appl Phys 1984;17:2139–2164.
34. Sedgewick SA, Trevena DH. Limiting negative pressure of water under dynamic stressing. J Phys D Appl Phys 1976;9:1983–1990.
35. Tomaru T, Geschwind HJ, Boussignac G, Lange F, Tahk SJ. Comparison of ablation efficacy of excimer, pulsed-dye, and holmium-YAG lasers relevant to shock waves. Am Heart J 1992;123:886–895
36. Chaussy Ch, Schmiedt E, Jocham D, Brendel W. First clinical experience with extracorporeally induced destruction of kidney stones by shock waves. J Urol 1982;127:217–220.
37. Kerr Muir MG, Sherrard ES. Damage to the corneal endothelium during Nd-YAG photodisruption. Br J Ophthalmol 1985;69:77–85.
38. Sverdrup A, Kjellsby E, Krüger PG, Fliysand R, Knudsen FR, Enger PS, Serck-Hanssen G, Helle KB. Effects of experimental seismic shock on vasoactivity of arteries, integrity of vascular endothelium and on primary stress hormones of the Atlantic salmon. J Fish Biol 1994;45:973–995.
39. Delius M, Enders G, Xuan Z, Liebich H-G, Brendel W. Biological effects of shock waves: kidney damage in dogs-dose dependence. Ultrasound Med Biol 1988;14:117–122.